Article

Not peer-reviewed version

Fibronectin- and Bioactive Glass-Modified Alginate Scaffolds Support Limited Primary Cell Proliferation In Vitro yet Demonstrate Effective Host Integration In Vivo

Benedetta Guagnini [†], Andrea Mazzoleni [†], Adrien Moya, Arnaud Scherberich, Barbara Medagli, Ivan Martin, Davide Porrelli [*], Manuele G. Muraro [*,‡], Gianluca Turco [‡]

Posted Date: 29 August 2025

doi: 10.20944/preprints202508.2185.v1

Keywords: alginate; fibronectin; bioactive glass; hydroxyapatite; bone scaffolds; mesenchymal stromal cells

Article

Fibronectin- and Bioactive Glass-Modified Alginate Scaffolds Support Limited Primary Cell Proliferation In Vitro yet Demonstrate Effective Host Integration In Vivo

Benedetta Guagnini [1,2,†], Andrea Mazzoleni [2,3,†], Adrien Moya [2], Arnaud Scherberich [2,3], Barbara Medagli [1], Ivan Martin [2,3], Davide Porrelli [4,*], Manuele G. Muraro [2,*,‡] and Gianluca Turco [1,‡]

[1] Department of Medicine, Surgery and Health Sciences, University of Trieste, Piazza dell'Ospitale 1, 34129, Trieste, Italy

[2] Department of Biomedicine, University of Basel and University Hospital of Basel, ZLF, Hebelstrasse 20, CH-4031, Basel, Switzerland

[3] Department of Biomedical Engineering, University of Basel, Hegenheimermattweg 167b, 4123 Allschwil, Switzerland

[4] Department of Life Sciences, University of Trieste, Via Alexander Fleming 31/B, 34127 Trieste, Italy

* Correspondence: dporrelli@units.it (D.P.); manuele.muraro@unibas.ch (M.G.M.); Tel.: +39-040-558-8894 (D.P.); +41-61-555-23-79 (M.G.M.)

† These authors contributed equally to the work.

‡ Co-last authors.

Abstract

Alginate-hydroxyapatite (AL) scaffolds modified with fibronectin (FN), or bioactive glass (BGMS10) have recently been characterized for their physicochemical properties and proposed as promising candidates for bone regeneration. Here, we present their first systematic biological evaluation, focusing on adhesion, proliferation, osteogenic differentiation in vitro, and in vivo host response. We compared FN-, BG-, and unmodified AL scaffolds using an immortalized mesenchymal stromal cell line (M-SOD) and primary human bone marrow-derived (BM-MSCs) and adipose-derived stromal cells (ASCs). FN scaffolds enhanced initial adhesion across all cell types and supported proliferation in M-SODs, while primary BM-MSCs and ASCs showed minimal expansion, regardless of scaffold type. BG scaffolds promoted expression of late-stage osteogenic markers in BM-MSCs, consistent with their ion release profile, but had limited impact on ASCs. In vivo subcutaneous implantation of acellular scaffolds in nude mice revealed robust host cell infiltration and extracellular matrix deposition across all scaffold types, confirming biocompatibility and integration. However, vascularization remained limited and did not differ substantially between formulations. Together, these findings highlight a critical discrepancy between immortalized and primary stromal cell response to scaffold cues, underscoring the challenge of sustaining primary cell proliferation in vitro. At the same time, the effective in vivo integration observed across scaffold types emphasizes the importance of host tissue responses for translational evaluation of functional biomaterials.

Keywords: alginate; fibronectin; bioactive glass; hydroxyapatite; bone scaffolds; mesenchymal stromal cells

1. Introduction

Developing advanced biomaterials for bone regeneration remains a central focus in tissue engineering, addressing the critical need for effective solutions to repair bone defects caused by

 doi:10.20944/preprints202508.2185.v1

trauma, congenital abnormalities, or degenerative diseases. An ideal scaffold must integrate seamlessly with the host tissue, mimic the bone's natural microenvironment, and provide structural support while promoting cellular proliferation and guiding stem cell differentiation into osteoblasts to achieve complete bone regeneration [1,2].

Among the various biomaterials available, alginate (Alg)—a biodegradable polysaccharide derived from brown seaweed—has been extensively utilized due to its biocompatibility, low toxicity, and gelation properties that support cell proliferation and nutrient diffusion [3]. However, its biological inertness, limited osteoconductivity, and poor mechanical strength present significant challenges, often necessitating modifications or the incorporation of bioactive components to enhance its functionality [4,5].

To address these limitations, hydroxyapatite (HAp), a mineral mimicking bone's inorganic matrix, was integrated to improve the scaffold's mechanical strength and also enhance osteoconductivity [6]. Subsequent investigations confirmed that Alg/HAp scaffolds significantly improve cellular interactions and mechanical properties, making them a promising candidate for bone regeneration [5,7,8]. Nonetheless, further optimization is required to fully exploit their osteogenic potential, as their composition, porosity, and bioactive signals critically influence differentiation and regeneration [9]. To enhance bioactivity two additional formulations were developed: one functionalized with fibronectin to improve cellular adhesion and proliferation, and another incorporating bioactive glass (BGMS10) [10], to stimulate osteogenesis and angiogenesis [11,12]. These formulations demonstrated enhanced bioactivity, biocompatibility, and structural properties, making them promising for bone regeneration.

However, immortalized cell lines often do not accurately reflect the complex behavior of primary cells, which are more physiologically relevant but exhibit distinct responses to biomaterial cues [13]. Furthermore, in vitro scaffold testing does not always predict in vivo outcomes [14], where host tissue interactions, immune response, and vascularization play critical roles in scaffold performance.

A crucial challenge in scaffold-based tissue engineering is bridging the gap between promising in vitro data and effective in vivo performance. Primary mesenchymal stromal cells (MSCs) and adipose-derived stromal cells (ASCs) are relevant candidates for bone regeneration due to their osteogenic potential and availability [15,16], respectively, but their interactions with these alginate-based scaffold compositions remain poorly understood. Additionally, while bioactive glass has been widely recognized for its osteoinductive properties [12], its efficacy in enhancing osteogenic differentiation in primary cell populations, particularly in comparison to other alginate-based formulations, remains to be fully characterized. Moreover, while in vitro studies focus on cellular responses in controlled environments, in vivo conditions introduce additional complexities, including scaffold degradation, host cell infiltration, and vascularization, which influence the long-term success of a biomaterial.

Based on these considerations, we hypothesize that scaffold composition significantly influences primary cell adhesion, proliferation, and osteogenic differentiation, with bioactive glass providing an advantage in osteogenic commitment. Furthermore, we hypothesize that scaffold structure and composition will impact early-stage host tissue integration in vivo, with potential cellular infiltration and remodeling differences over time.

To test these hypotheses, we evaluated three scaffold formulations, Alg/HAp (AL), Fibronectin-Alg/HAp (FN), and BGMS10-Alg/HAp (BG), for their ability to support adhesion, proliferation, and osteogenic differentiation of primary MSCs and ASCs. In parallel, we implanted acellular scaffolds subcutaneously in immunodeficient mice to gain preliminary insights into host-material interactions, cellular infiltration, and early extracellular matrix deposition.

This study is, to our knowledge, the first to directly compare the responses of primary BM-MSCs and ASCs with those of an immortalized mesenchymal cell line on these functionalized AL scaffolds, and to assess both in vitro outcomes and in vivo host tissue integration within the same scaffold system. By combining primary cell assays with ectopic implantation, we reveal scaffold-specific

 doi:10.20944/preprints202508.2185.v1

limitations in proliferation and differentiation support, and explore the potential of the host environment to overcome them. This dual approach addresses a critical gap in scaffold evaluation pipelines, where primary human cell testing and in vivo integration studies are rarely performed in tandem.

2. Materials and Methods

2.1. Culture Media

Three culture media formulations were used in this study: complete medium (CM), proliferation medium (PM), and osteoblastic differentiation medium (OB). The CM was composed of α-Modified Eagle's Medium (α-MEM) supplemented with 10% fetal bovine serum (FBS), 2 mM GlutaMAX, 100 mM HEPES, 1 mM sodium pyruvate, 100 U/mL penicillin, 100 µg/mL streptomycin, and 5 ng/mL fibroblast growth factor-2 (FGF2). The PM (DAF medium) was prepared by supplementing CM with 10 nM dexamethasone, 0.1 mM ascorbic acid, and 5 ng/mL FGF2. The OB medium was obtained by enriching CM with 1 µM dexamethasone, 0.1 ascorbic acid, and 10 mM beta-glycerophosphate. Table S1 provides full details on all reagents used in this study, including catalog numbers.

2.2. Cell Source and Expansion

Bone marrow (BM) aspirates were obtained during routine orthopedic surgical procedures involving iliac crest exposure, while human adipose tissue samples were collected from patients undergoing liposuction or abdominoplasty. Informed consent was obtained under the general consent (Forschungskonsent) of the University Hospital Basel, approved by Swissethics (Art. 29, 32 Human Research Ordinance, HFV).

Freshly isolated BM nucleated cells were plated at 1×10^5 cells/cm^2 in CM, with medium changes twice per week. Upon confluence, BM-derived mesenchymal stromal cells (hBM-MSCs) were expanded at $3–5\times10^3$ cells/cm^2. Cells at passage 2 or 3 (p2–p3) were enzymatically detached using 0.05% trypsin/0.01% EDTA, counted, and used for 3D culture. Immortalized M-SOD (Mesenchymal Stromal Cells Sword of Damocles) cells were expanded in CM before seeding at p6, following Bourgine et al. [17].

Stromal vascular fraction (SVF) cells were isolated from adipose tissue via enzymatic digestion.16 The resulting cells were seeded at 2×10^4 cells/cm^2 and expanded for one week. The adherent population, adipose-derived stromal cells (ASCs) p0, was detached with 0.05% trypsin/0.01% EDTA, reseeded at 3×10^3 cells/cm^2, and further expanded to p1. A total of 5×10^5 ASCs at p1 were used for experiments [18,19].

2.3. Materials and Scaffold Manufacturing

Sodium alginate (MW = 135,000, FG = 0.67; FGG = 0.59), derived from Laminaria Hyperborea, was obtained from FMC Biopolymers (Drammen, Norway). Hydroxyapatite (HAp), bioactive glass (BGMS10), glucono-delta-lactone (GDL), and fibronectin (1 mg/mL) were purchased from Merck KGaA. Alginate/Hydroxyapatite scaffolds (AL) were fabricated following the protocol of Turco et al. [6], with BGMS10 bioactive glass incorporation (BG) and fibronectin functionalization (FN) prepared as described by Guagnini et al. [12] and Zumbo et al. [11], respectively. Briefly, a 2% (w/v) alginate and 3% (w/v) HAp suspension was mixed with 60 mM GDL, cast into molds, and left to gel overnight. Scaffolds were cryopreserved, freeze-dried, and sectioned into uniform 10 mm × 3 mm cylinders using a 3D-printed polylactic acid (PLA) slicer (Figure S1). For in vivo implantation, scaffolds were trimmed to 4 mm × 3 mm. Sterilization was performed via UV light (90 min), then deionized water washing and antibiotic treatment. Before use, AL and BG scaffolds were equilibrated in culture media for 24 hours, while FN-coated scaffolds were pre-incubated in 10 µg/mL fibronectin solution for 24 hours before equilibration.

The physicochemical and mechanical properties of these scaffolds have been extensively characterized in the cited studies, using identical raw materials and fabrication protocols. AL

 doi:10.20944/preprints202508.2185.v1

scaffolds exhibit >88% interconnected porosity with pores of 100–300 μm, a dry compressive modulus of ~6.3 MPa and ultimate strength of ~0.29 MPa, and a hydrated modulus of ~83 kPa. Incorporation of BGMS10 slightly reduces porosity (80.2 ± 1.1% at 0.3% w/v BG; 70.2 ± 0.6% at 0.6% w/v BG) and maintains comparable dry-state mechanical properties, while contributing ion release (Si, Ca, Na, P, Mg, Sr) known to stimulate osteogenesis. Fibronectin functionalization forms a thin, stable surface coating confirmed by μBCA assay, enhancing cell adhesion without altering scaffold morphology. Key parameters from the original characterization are summarized in Supplementary Table S2.

2.4. Adhesion and Proliferation

Scaffolds were tap-dried on sterile gauze for 5 seconds, transferred to a 24-well plate, and seeded with 1×10^6 cells in 100 μL of complete medium (CM). After incubation at 37°C in a humidified 5% CO_2 atmosphere for 3 hours to facilitate attachment, 1.5 mL of CM was carefully added per well, and scaffolds were maintained with medium changes every 3 days. Seeding efficiency and proliferation were assessed at 24 hours and 7 days post-seeding using MTT and CellTiter-Glo assays. Seeding efficiency was calculated by comparing scaffold-attached cells at 24 hours to 2D controls (100% retention). The proliferation rate was determined by comparing the 7-day signal to the 24-hour 2D culture reference, indicating net cell expansion. For MTT assays, scaffolds were incubated with 700 μL of MTT solution (1 mg/mL) for 3 hours at 37°C in the dark. Formazan crystal formation was observed under an EVOS XL Core microscope to assess cell distribution, followed by solubilization in dimethyl sulfoxide (DMSO) and absorbance measurement at 560 nm. Cell-free scaffolds served as blanks. Additionally, the CellTiter-Glo Luminescent Assay was performed following the manufacturer's protocol to quantify ATP levels, with results in the supplementary data.

2.5. Scanning Electron Microscopy (SEM)

Scanning Electron Microscopy (SEM) was used to analyze the surface morphology and microstructure of the scaffolds. After culture, samples were fixed overnight at 4°C in 0.1 M sodium cacodylate buffer with 2% glutaraldehyde, followed by dehydration through a graded ethanol series (30–100%; 15 min per step) and critical point drying (Autosamdri-815, Tousimis). Dried samples were mounted on aluminum stubs, sputter-coated with a 20 nm gold layer (LEICA EM Ace 600), and imaged using a ZEISS Gemini 2 scanning electron microscope at 5 kV primary electron beam voltage and 200 pA probe current, with magnifications ranging from 50× to 5000×. Longitudinal and transversal sections were qualitatively assessed for microstructural features.

2.6. RNA Extraction and Quantitative Real-Time PCR

Total cellular RNA was extracted using TRI Reagent solution combined with the Qiagen Miniprep Kit, following mechanical homogenization with the FastPrep-24 lysis system and stainless steel beads. RNA concentration and purity were assessed using a NanoDrop ND-1000 spectrophotometer. For cDNA synthesis, 1 μg of RNA was reverse-transcribed using SuperScript III reverse transcriptase, following the manufacturer's protocol. Quantitative real-time PCR (qRT-PCR) was performed using the ViiA 7 Real-Time PCR System with TaqMan Gene Expression Assays. Gene expression levels for Runt-related transcription factor 2 (RUNX2), Osteocalcin (BGLAP), Ki-67, Osteopontin (OPN), Bone Sialoprotein (BSP), Collagen type I (COL1A1), and Alkaline Phosphatase (ALP) were normalized to GAPDH and analyzed using the 2-ΔΔCT method to calculate fold changes relative to the control condition.

2.7. Whole Mount Immunostaining and Confocal Imaging

Tissue constructs were fixed overnight in 4% PFA at 4°C, rinsed in PBS, and permeabilized with 0.4% Triton X-100 in PBS (PBS-T) for 10 min. Non-specific binding was blocked with 5% goat serum in PBS-T for 1 hour. For DAPI-Phalloidin-Ki67 staining, constructs were incubated overnight at 4°C in a blocking buffer containing FITC-Phalloidin and rat anti-human Ki-67 primary antibody (1:500).

 doi:10.20944/preprints202508.2185.v1

After PBS washes, samples were incubated for 4 hours at room temperature with goat anti-rat Alexa Fluor 647 secondary antibody (1:1000). Nuclei were counterstained with DAPI (1:1000) for 10 min. Samples were mounted onto multiwell imaging slides and imaged using a Nikon AXR confocal microscope.

2.8. In Vivo Ectopic Implantation in Nude Mice

Given the limited adherence and proliferation of primary cells observed in vitro, we elected to perform acellular subcutaneous implantation to evaluate scaffold colonization by host-derived cells and early extracellular matrix deposition. This model allowed us to isolate host–material interactions, independent of donor cell viability, and to adhere to the 3R principle by avoiding more invasive orthotopic models at this exploratory stage. The results were intended to provide a first validation of scaffold compatibility before advancing to critical-size bone defect models. Acellular scaffolds were subcutaneously implanted in Rj:NMRI-Foxn1<nu/nu> female nude mice (Janvier Labs, Le Genest-Saint-Isle, France). All animal procedures were conducted under the approval of the Cantonal Veterinary Office of Basel-Stadt (permit number BS 1797, and National no. 37404), in accordance with the Swiss Animal Welfare Act (TSchG, SR 455) and Ordinance (TSchV, SR 455.1), and in compliance with the 3Rs principles. The implantation protocol followed the procedure described by Osinga and colleagues [20].

2.9. Histological Processing and Staining

After differentiation or explantation, scaffolds were rinsed in PBS and fixed overnight in 4% paraformaldehyde (PFA) at 4°C. For structural support, samples were embedded in HistoGel before paraffin embedding. Using a Thermo Scientific HM 355S microtome, 10 µm thick sections were cut and mounted onto SuperFrost Plus slides. Sections were deparaffinized, rehydrated, and stained to assess tissue morphology, mineralization, and extracellular matrix composition.

For Hematoxylin and Eosin (H&E) staining, sections were stained with hematoxylin (nuclei, blue) and eosin (cytoplasm, pink) to evaluate general morphology. Calcium deposition was assessed via Alizarin Red staining, where rehydrated sections were incubated in 1% Alizarin Red solution (pH 4.2) for 30 sec and then thoroughly rinsed in distilled water. Mineralized regions appeared red-orange under light microscopy. Collagen deposition and tissue organization were analyzed using Masson's Trichrome staining, where collagen fibers stained blue, cytoplasm/muscle fibers red, and nuclei dark brown/black. Stained sections were imaged using a Hamamatsu Nanozoomer S60 slide scanner.

2.10. Immunofluorescence Staining

Scaffold sections were deparaffinized in Ultraclear (3×15 min), rehydrated through a descending ethanol series, and rinsed in distilled water. Antigen retrieval was performed in a citrate buffer (pH 6) at 96°C for 15 min, then cooling and PBS washes. Sections were blocked for 30 min in 5% animal serum in PBS-T (0.2%) to prevent non-specific binding.

Primary antibodies, rat anti-mouse CD31 (1:200) and rabbit anti-human Vimentin (1:200), were diluted in 1% serum in PBS-T and incubated overnight at 4°C. After PBS-T and PBS washes, secondary antibodies, AlexaFluor 647 anti-Rat (1:400) and AlexaFluor 546 anti-Rabbit (1:400), were applied for 30 min at room temperature. Nuclei were counterstained with DAPI (1:500) for 10 min, and sections were mounted in Fluoromount Aqueous Mounting Medium before drying in the dark.

Immunofluorescence images were captured using a Nikon Ti2 widefield microscope equipped with a Nikon DS-Ri2 camera, CFI Plan Apo Lambda NA 0.75×, 20× objective, and NIS-Elements AR 5.21.03 software.

2.11. Statistical Analysis

Statistical analyses were performed using GraphPad software (version 8.0.2). Data normality was assessed using the Shapiro–Wilk test. For normally distributed datasets, one-way ANOVA with

 doi:10.20944/preprints202508.2185.v1

Bonferroni's correction was applied. Kruskal–Wallis and Mann–Whitney U tests were used for non-normally distributed data, both with Bonferroni's correction. A p-value of $\alpha = 0.05$ was considered statistically significant. For comparisons between two groups with unequal variances, Welch's t-test was used instead of a standard t-test, as it does not assume equal variances and is more robust in cases of variance heterogeneity.

3. Results

A sequential approach was employed to evaluate the performance of alginate-based composite scaffolds, as outlined in Figure 1. We first assessed cell adhesion and proliferation using M-SOD and primary mesenchymal stromal cells in vitro, followed by osteogenic differentiation studies. Finally, scaffold integration was examined in vivo using a subcutaneous ectopic model in mice.

Cell adhesion and proliferation were first assessed in vitro (Figure 2), revealing scaffold-dependent differences in stromal cell interaction. These were followed by osteogenic differentiation studies and in vivo implantation to evaluate tissue integration (Figure 3–5).

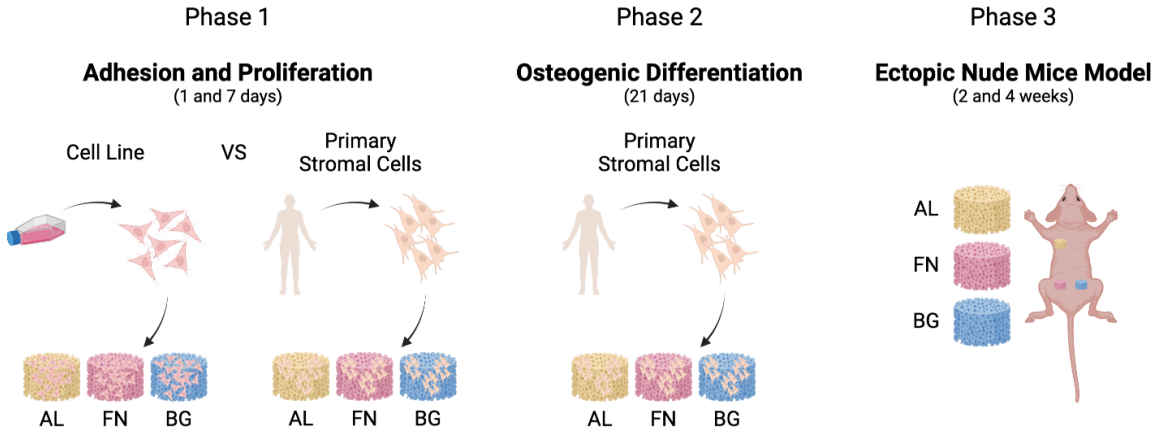

Figure 1. Schematic representation of the Study Design. AL: Alginate/Hydroxyapatite, FN, Alginate/Hydroxyapatite-Fibronectin, BG: Alginate/Hydroxyapatite-BGMS10. Cell Line: MSOD, Primary Stromal Cells: BM-MSCs, and ASCs. Created in BioRender. Martin, I. (2025) https://BioRender.com/hfr1iqk.

3.1. Fibronectin Promotes MSC and ASC Adhesion and Growth, While Bioactive Glass Has Minimal Impact

The adhesion and proliferation of stromal cells on three scaffold formulations—Alg/HAp (AL), fibronectin-functionalized (FN), and BGMS10-incorporated (BG)—were assessed using MTT assays and SEM imaging (Figure 2). Bone marrow-derived mesenchymal stromal cells (BM-MSCs), adipose-derived stromal cells (ASCs), and immortalized M-SOD cells exhibited distinct interactions with the scaffolds.

FN-functionalized scaffolds significantly improved seeding efficiency for all cell types on Day 1 compared to AL scaffolds (Figure 2A), highlighting the role of FN in promoting initial cell adhesion, particularly for MSCs. In contrast, BG scaffolds did not significantly enhance seeding efficiency over AL scaffolds, suggesting that bioactive glass alone does not provide additional adhesion cues for primary cells. The observed adhesion trends were further examined using MTT staining (Suppl. Figure 2), which showed higher signal intensity in FN scaffolds, potentially reflecting more significant metabolic activity in viable cell clusters. While all scaffolds demonstrated biocompatibility, ASCs exhibited greater MTT conversion, suggesting higher metabolic activity. However, since MTT only reflects metabolic function, this does not necessarily indicate improved adhesion efficiency or long-term proliferation.

Proliferation rates varied across different cell types and scaffold formulations. Immortalized M-SOD cells exhibited significantly higher proliferation than primary BM-MSCs and ASCs on all scaffolds from Day 1 to Day 7 (Figure 2B), consistent with previous studies on MG-63 osteosarcoma

 doi:10.20944/preprints202508.2185.v1

cells [11,12]. This highlights the inherently greater proliferative capacity of immortalized cell lines in scaffold studies. In contrast, primary BM-MSCs and ASCs showed minimal proliferation across all conditions, underscoring the challenges of sustaining primary cell expansion on these formulations. FN scaffolds slightly improved metabolic activity and retention for primary cells, but this did not translate into a significant proliferation increase. These findings reinforce the role of fibronectin in supporting initial cell attachment, though additional strategies may be required to enhance long-term primary cell growth.

SEM imaging (Figure 2C) provided critical insights into cell morphology and scaffold interactions. On AL scaffolds, cells predominantly exhibited a spherical morphology with limited adhesion, reinforcing alginate's poor intrinsic bioactivity. In contrast, FN scaffolds supported well-spread and flattened cells, particularly ASCs, indicating strong adhesion and engagement with the scaffold surface. BG scaffolds presented a mix of rounded and partially spread cells, suggesting moderate adhesion, though not to the extent observed in FN scaffolds. Notably, some primary cells on AL scaffolds (Figure 2C, d-f) displayed signs of cellular stress, including membrane rupture (red arrows), highlighting the limitations of alginate as a biologically inert material.

Together, these results show that FN functionalization significantly improves cell adhesion and retention, while BG alone does not enhance early cell-scaffold interactions. These findings highlight the importance of scaffold bioactivity in promoting initial cell attachment, especially for primary stromal cells, though additional strategies may be required to support long-term proliferation.

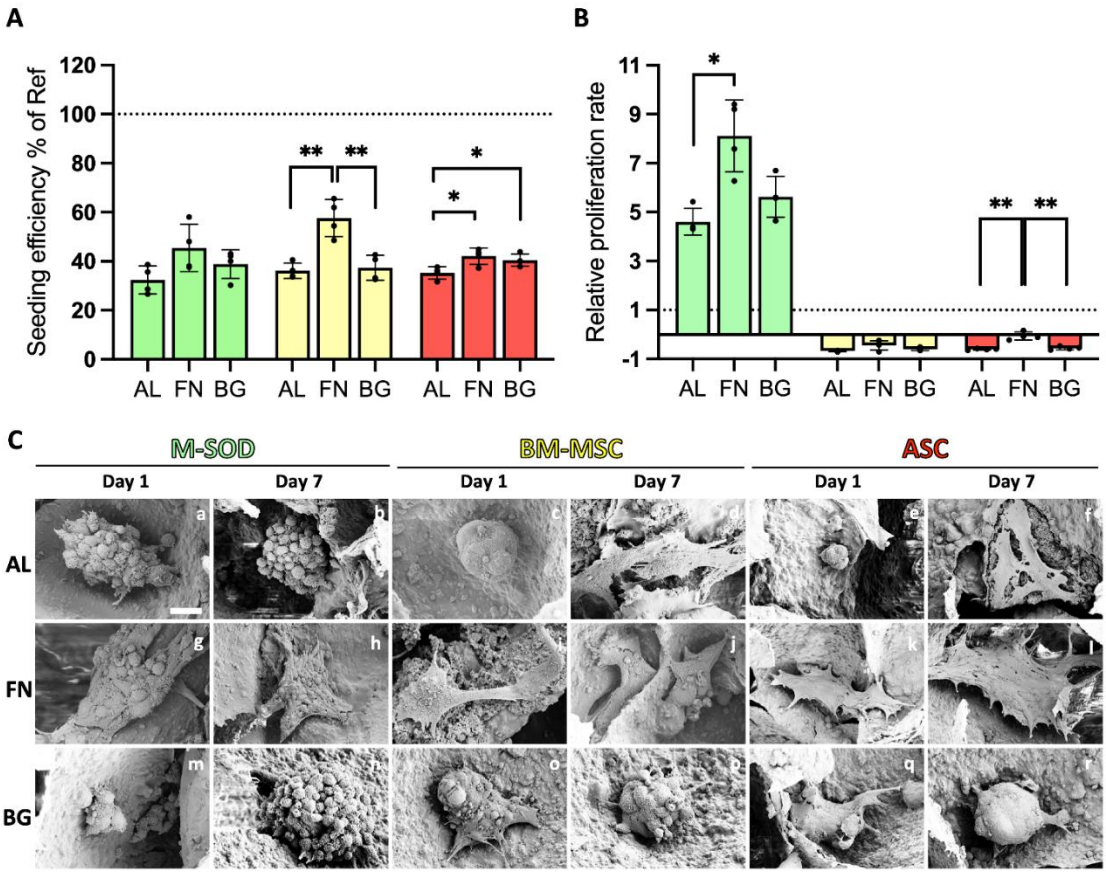

Figure 2. Seeding efficiency, proliferation, and cell morphology of cells on scaffolds. M-SOD (green), BM-MSCs (yellow), and ASCs (red) on AL, FN, and BG scaffolds, assessed via MTT assays and SEM. (A) Seeding efficiency at Day 1, expressed relative to 2D well-plate controls (dashed line at 100%). (B) Relative proliferation rate from Day 1 to Day 7, normalized to Day 1 values (dashed line at 1 on the Y-axis). Error bars represent standard deviation from quadruplicate measurements. Statistically significant differences are indicated ($p < 0.01$). (C) SEM images of M-SOD, BM-MSCs, and ASCs on AL, FN, and BG scaffolds on Day 1 and Day 7, illustrating cell morphology and scaffold interaction. Scale bars = 10 μm.

 doi:10.20944/preprints202508.2185.v1

3.2. Scaffold Composition Influences Osteogenic Differentiation: BG Supports BM-MSCs, ASCs Remain Undifferentiated

Following the assessment of adhesion and proliferation, we evaluated the osteogenic differentiation potential of BM-MSCs and ASCs cultured on AL, FN, and BG scaffolds. Gene expression analysis of key osteoblastic markers (RUNX2, COL1A1, ALP, OPN, BSP, BGLAP) was performed via RT-qPCR after 21 days in osteogenic conditions to assess the impact of scaffold composition on differentiation (Figure 3A). BM-MSCs (top row) exhibited scaffold-dependent differentiation patterns. While RUNX2 expression remained unchanged across conditions, COL1A1 expression was significantly higher on AL and BG scaffolds, suggesting that these formulations promote extracellular matrix deposition. This could be attributed to the stiffer nature of AL and BG scaffolds, which may provide mechanical cues for matrix synthesis. Notably, late-stage osteogenic markers (ALP, OPN, BSP, BGLAP) were significantly upregulated in BM-MSCs cultured on BG scaffolds, indicating a more advanced osteogenic maturation. This suggests that BG scaffolds enhance osteogenic differentiation, likely due to bioactive ion release that promotes cellular commitment to the osteoblastic lineage. In contrast, ASCs (bottom row) displayed minimal osteogenic differentiation across all scaffold types. While COL1A1 expression was elevated on AL and BG, late-stage osteogenic markers (BSP, BGLAP, ALP) were undetectable, suggesting that ASCs lack the intrinsic cues for osteogenic commitment.

SEM analysis (Figure 3B) revealed compact, rounded cell clusters in BM-MSCs and ASCs across all scaffold types, with no substantial morphological differences. This suggests that, despite variations in gene expression, cellular organization remains essentially unchanged.

These findings reinforce that scaffold composition plays a key role in osteogenic differentiation. BG scaffolds support BM-MSC maturation, while ASCs require additional cues to fully commit to the osteogenic lineage.

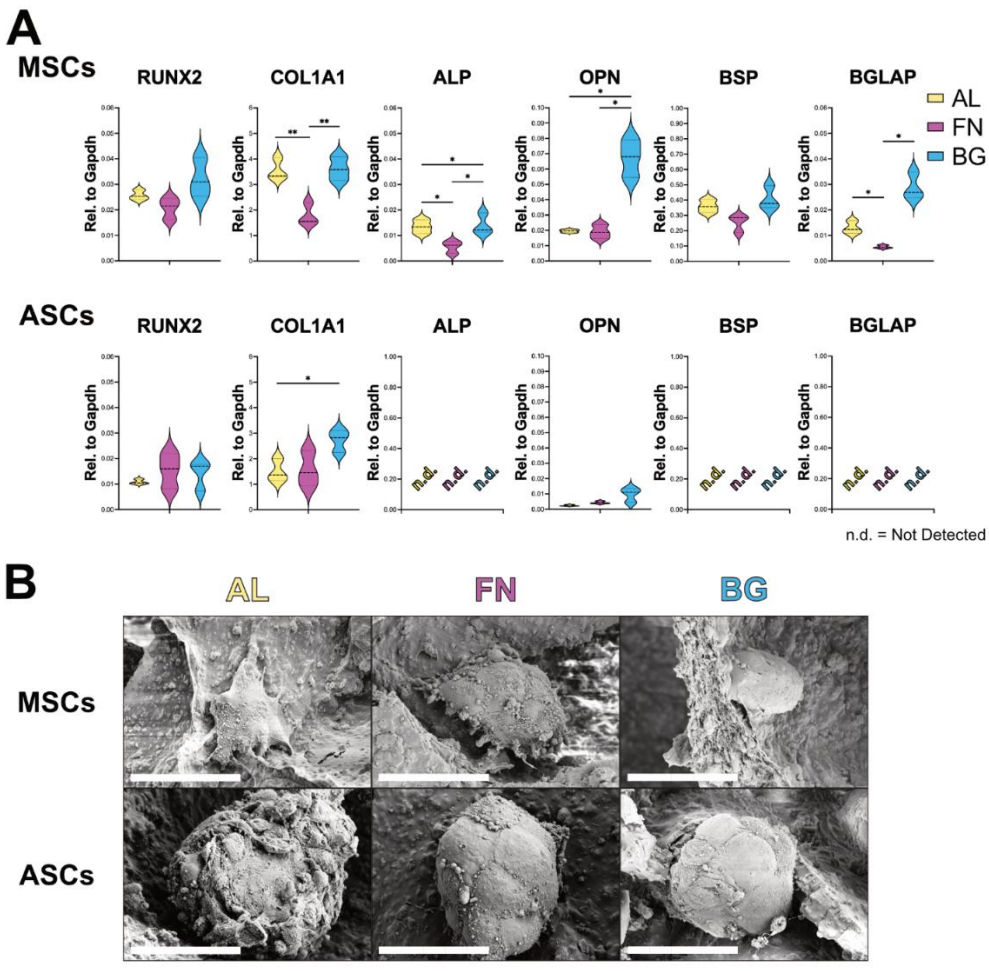

 doi:10.20944/preprints202508.2185.v1

Figure 3. Osteogenic differentiation of BM-MSCs and ASCs on AL, FN, and BG scaffolds. (A) Gene expression levels of RUNX2, COL1A1, ALP, OPN, BSP, and BGLAP in BM-MSCs (top) and ASCs (bottom) after 21 days in osteogenic media. Results represent mean ± SD from three scaffolds per formulation. n.d. = not detected. Statistically significant differences are indicated ($p < 0.05$; $p < 0.01$). (B) SEM images of BM-MSCs and ASCs on AL, FN, and BG scaffolds after 21 days in osteogenic media. High-magnification SEM images show the compact, spherical morphology of cell clusters interacting with the scaffold surface. Scale bars = 50 μm.

3.3. Scaffold Stability and Cells Morphology in Long-Term Culture

In addition to assessing cell morphology, we also examined the long-term structural stability of the scaffolds. Assessing scaffold structural integrity over time is crucial before in vivo implantation, as material degradation can affect tissue integration. To evaluate this, we analyzed the microstructural stability of AL, FN, and BG scaffolds after 28 days in culture using SEM imaging (Figure 4). The SEM images reveal that the inner scaffold network (top row) maintained its interconnected porosity, indicating sustained structural integrity under osteogenic conditions. Additionally, higher-magnification images (bottom row) highlight that surface texture and pore structure remained unchanged, reinforcing the stability of AL, FN, and BG scaffolds. These findings are consistent with previous studies [8,11], which reported scaffold stability for up to 14 days under different culture conditions. Our results extend this observation, demonstrating that these scaffold formulations can maintain their architecture for at least 28 days in culture, further supporting their potential for long-term bone tissue engineering applications. Beyond scaffold integrity, cellular morphology was examined in greater detail to further assess how different scaffold formulations influence cell behavior over prolonged culture periods (Figure 4B-C). Consistent with previous observations, BM-MSCs and ASCs exhibited similar morphologies across all scaffold formulations, predominantly forming compact spheroid-like clusters. These findings reinforce the earlier structural analysis, confirming that scaffold composition does not significantly impact long-term cell morphology.

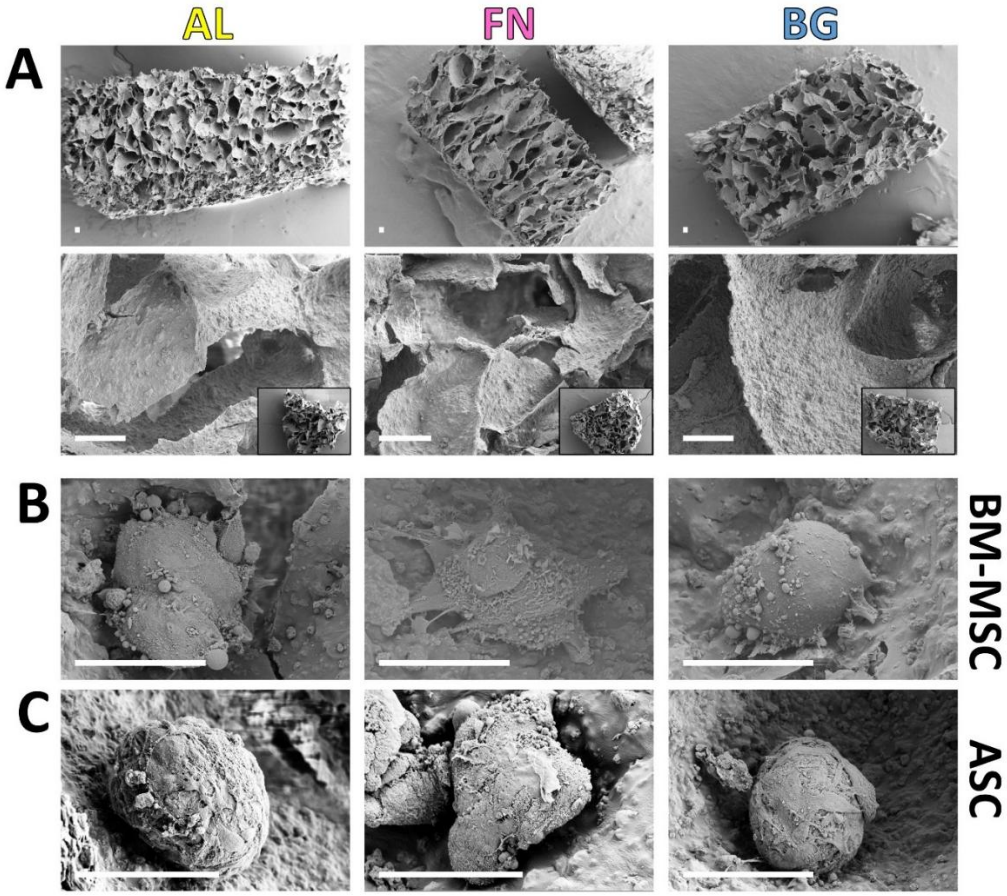

 doi:10.20944/preprints202508.2185.v1

Figure 4. Scaffold Structural Integrity and Cells Morphology on Alginate-Based Scaffolds After Long-Term Culture. A (top row): SEM images of AL, FN, and BG scaffold cross-sections after 28 days in culture show preserved porous architecture with no visible signs of degradation or collapse. High-magnification SEM images (A, bottom row) of scaffolds highlight the surface texture and pore structure. Insets show the entire scaffold structure at a lower magnification. Scale bars: 100 μm. BM-MSCs (B) and ASCs (C) interacting AL, FN, BG scaffolds, confirming the compact, round morphology of cell clusters and their interaction with the scaffold surface. Scale bars: 50 μm.

3.4. Alginate-Based Scaffolds Support Early Cell Infiltration and Collagen Deposition, But Lack Vascularization

Histological and ultrastructural analyses were performed after 2 and 4 weeks of subcutaneous implantation to assess host cell infiltration and ECM deposition (Figure 5). H&E staining confirmed that all scaffolds supported host cell invasion, with an increase in cellular density over time. No major differences in cell distribution were observed among AL, FN, and BG scaffolds, indicating comparable tissue integration. Masson's Trichrome staining revealed progressive collagen deposition, with FN scaffolds showing the earliest signs of fibrillar network formation. By 4 weeks, ECM accumulation increased across all scaffold types, though FN scaffolds exhibited a more structured matrix, while BG scaffolds showed a less organized collagen distribution.

SEM analysis further confirmed that all scaffolds remained structurally intact and exhibited increasing ECM deposition over time. While FN scaffolds displayed a denser fibrillar network, no strong material-dependent differences in scaffold remodeling were observed.

These findings demonstrate that all biomaterials tested were successfully invaded by host cells, supporting their basic biocompatibility. However, due to the lack of quantification and limited sample sizes, no conclusions can be drawn regarding differential scaffold performance, therefore further studies are needed to comprehensively evaluate their long-term integration and functional potential.

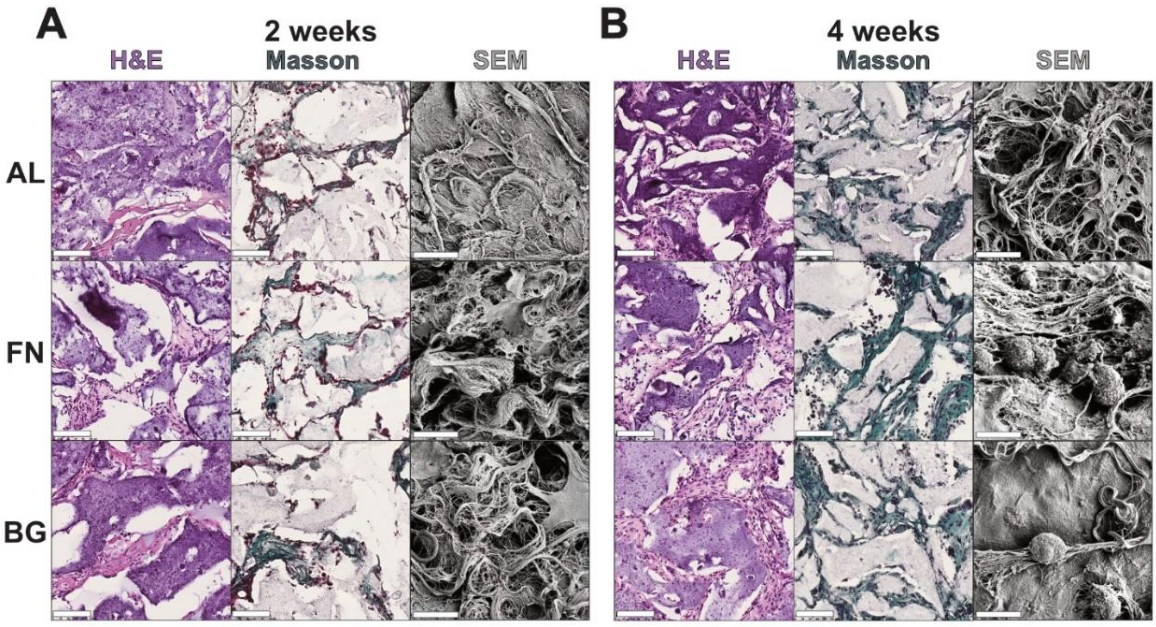

Figure 5. Histological Analysis of Scaffolds Post 2 and 4-Weeks Subcutaneous Implantation. H&E staining shows cell infiltration and tissue integration, with nuclei appearing dark purple and cytoplasm and extracellular matrix staining light pink. Masson's Trichrome staining confirms cell nuclei (purple) and highlights collagen deposition in green, indicating tissue remodeling and scaffold integration. Insets display low-magnification overviews of entire scaffold sections. Scale bars represent 500 μm.

 doi:10.20944/preprints202508.2185.v1

The immunofluorescence (IF) staining (Figure S2) presents a comparative evaluation of cellular infiltration and vascularization within the four scaffold formulations (AL, FN, BG) after 4 weeks of subcutaneous implantation. Each scaffold is stained for DAPI (nuclear marker), Vimentin (Vim; mesenchymal cell marker), and CD31 (endothelial cell marker). Vimentin staining confirmed stromal cell infiltration across all scaffold types, with no significant differences in distribution or density between AL, FN, and BG scaffolds, suggesting a comparable ability to support mesenchymal cell invasion, confirming our previous results (Figure 5). CD31-positive regions were observed within the scaffold structures (Figure S3). However, the signal was relatively weak and appeared to overlap with scaffold architecture in some areas, raising the possibility of non-specific staining or autofluorescence from the material. CD31-positive regions were detected across all scaffold types, but the signal appeared weaker in FN scaffolds compared to AL and BG, suggesting a potentially lower presence of endothelial cells in FN scaffolds. Given these limitations, the current data are provided as Figure S3 for transparency but are not used to draw definitive conclusions about scaffold vascularization.

4. Discussion

Developing biomaterials for bone tissue engineering requires a translational approach that integrates in vitro characterization with in vivo assessment to evaluate scaffold biocompatibility, integration, and resorption. While many studies rely on immortalized cell lines for initial screening, primary mesenchymal stromal cells (MSCs) and adipose-derived stromal cells (ASCs) provide a more physiologically relevant model, capturing interpatient variability and more accurately reflecting clinical conditions [21]. As summarized in Table S2 (adapted from refs 11 and 12) alginate/hydroxyapatite (AL) functionalized with fibronectin (FN) or incorporating bioactive glass (BG) has previously been shown to enhance the biocompatibility of AL scaffolds with respect to the human osteosarcoma cell line (MG-63). Due to their structural characteristics, these scaffolds are promising candidates for supporting cellular activity and tissue integration in bone regeneration.

Here, we demonstrated that the scaffolds were effective for adhesion and proliferation using an immortalized bone marrow-derived mesenchymal stem cell line (M-SOD). However, when testing with bone marrow-derived and adipose-derived primary mesenchymal cells, although adhesion remained strong, we observed no cell proliferation. Furthermore, we could demonstrate osteoblastic differentiation only with MSCs, while this was limited to ASCs. Although ASCs are known to be less effective for osteogenic differentiation, this finding highlights the need for optimized biochemical cues tailored to specific cell populations. Nevertheless, we also confirmed in primary cells the inherent biological inertness of AL scaffolds that limited cell adhesion and proliferation. This aligns with previous studies reporting alginate's inability to provide the biochemical cues necessary for robust cellular interaction.9 Fibronectin-functionalized scaffolds (FN) improved cell adhesion, particularly with MSCs, confirming the critical role of fibronectin in enhancing integrin-mediated cellular attachment and spreading [22]. These findings support previous evidence that fibronectin coatings can enhance scaffold surfaces to create a more physiologically supportive environment for cell activity [23]. In contrast, BG scaffolds did not significantly affect initial cell attachment compared to AL scaffolds, indicating that the inclusion of BGMS10 does not immediately improve cell attachment. However, this may be because bioactive glasses need longer cultures to boost cell activity [9,24,25]. Indeed, after 21 days of osteogenic differentiation, the BG scaffolds exhibited higher expression of gene markers associated with mature osteoblasts. This increased expression is likely driven by the release of magnesium and strontium ions from BGMS10. Magnesium aids stem cell differentiation and strengthens newly formed bone, while strontium enhances osteoblast activity and inhibits osteoclast-mediated resorption, resulting in increased bone mass and strength [26,27]. These effects are consistent with the ion release profile of BGMS10 scaffolds (Supplementary Table S2), which includes Si, Mg, and Sr ions known to promote osteogenesis [12]. However, both cell types, MSCs and ASCs, primarily formed compact, rounded cell clusters across all scaffold formulations, demonstrating limited cell spreading. This spherical morphology indicates that the bioactive cues

 doi:10.20944/preprints202508.2185.v1

provided were insufficient to create an optimal environment for cellular colonization. The 28 days of culture required for the osteogenic differentiation assay also allowed for the observation that these scaffold architectures were preserved, supporting their potential for long-term bone tissue engineering applications. This observation was further confirmed in vivo experiment.

While gene expression profiling provided valuable insights into osteogenic commitment, additional endpoint assays such as mineral deposition or immunostaining for late-stage osteogenic markers were not feasible in the present setup. The high hydroxyapatite content of the scaffolds precluded Alizarin Red-based quantification, and histological processing of in vitro cultured scaffolds was hindered by poor adherence to glass slides. These limitations emphasize the value of our parallel in vivo analysis, which allowed assessment of tissue infiltration and extracellular matrix deposition under physiological conditions. Future studies will build on these findings with alternative strategies to enable complementary marker analysis.

For biomaterial characterization targeting future clinical applications, it is essential to evaluate how alginate porous scaffolds perform in a physiological environment [28,29]. In this study, we selected a subcutaneous acellular implantation model because in vitro experiments showed minimal primary cell proliferation, making it premature to implant cell-seeded constructs. This choice allowed us to focus on early host-material interactions and tissue infiltration under physiological conditions, while also respecting the 3R principle by avoiding more invasive orthotopic bone defect models at this stage. While orthotopic implantation in a critical-size bone defect would provide a more specific evaluation of the scaffolds' osteogenic potential, this method aimed to investigate the initial interaction between the scaffolds and host tissue in a simpler in vivo model [30]. Subcutaneous models are frequently used for initial biocompatibility screening and for assessing the tissue response to implanted biomaterials [31]. After four weeks, none of the tested biomaterials were reabsorbed and were effectively infiltrated by host cells despite alginate's biological inertness in vitro. The lack of significant differences between the scaffolds in cellular density and collagen deposition suggests that modifications with fibronectin and bioactive glass did not significantly alter the host response at this early stage. While ECM formation was evident, additional characterization is required to determine its organization and functional role in scaffold remodeling. Previous studies have underscored the importance of a well-formed ECM in facilitating sustained tissue remodeling and mechanical strength in bone regeneration [32].

Another important finding was the low expression of CD31, an endothelial marker, across all scaffolds. This suggests that vascularization remains a significant challenge, particularly for BG scaffolds, where angiogenic stimulation induced by the presence of Mg^{2+} and Sr^{2+} is expected [33]. These ions are part of the BGMS10 ion release profile (summarized in Supplementary Table S2), which includes Mg, Sr, and Si, all reported to contribute to osteogenic and angiogenic signaling [12]. Assessing the bioavailability of those ions in vivo will shed light on those results, and eventually addressing this issue in future studies by co-delivering pro-angiogenic factors (e.g., VEGF) or utilizing pre-vascularization strategies in dynamic culture systems could significantly enhance both osteogenic and angiogenic outcomes in vivo [34,35].

Given these findings, future in vivo studies should transition to orthotopic implantation models (e.g., mouse calvarial or femoral defect models) to assess long-term scaffold integration, bone formation, and vascularization under physiologically relevant conditions [36].

5. Conclusions

This study highlights the importance of integrating primary cell testing and in vivo evaluation for optimizing alginate-based composite scaffolds in bone tissue engineering. While fibronectin improved adhesion, it did not enhance osteogenesis. Bioactive glass scaffolds promoted osteogenic differentiation in MSCs but showed limited cell proliferation and spreading.

Scaffolds showed host cell infiltration compatibility in our in vivo follow-up study, with mouse cells establishing a hold and depositing ECM regardless of scaffold composition. This demonstrated scaffold biocompatibility despite inherent alginate inertness. The observed low vascularization in

 doi:10.20944/preprints202508.2185.v1

vivo shows that challenges remain to scaffold integration and clinical translation. Future work should be focused on biochemical scaffold modification aimed at vascularization enhancement. Provided vascular integration in the scaffolds, orthotopic implantation models would be required to truly assess the constructs in a physiologically relevant setup. By addressing these challenges, alginate-based scaffolds hold promise for bridging the gap between in vitro potential and in vivo efficacy.

Supplementary Materials: The following supporting information can be downloaded at: https://www.mdpi.com/article/doi/s1, Figure S1: Scaffold Manufacturing Process Using 3D-Printed PLA Slicer; Figure S2: Light Microscope Images Showing Cells Adhesion and Distribution; Figure S3: Vascularization of scaffolds post 4 weeks implantation; Table S1: Details and catalogs numbers of reagents used in this study; Table S2: Physicochemical and mechanical properties of scaffold formulations.

Author Contributions: Conceptualization, B.G. A.M.1, A.M.2, A.S., I.M., M.G.M.; Data curation, B.G., A.M.1, M.G.M.; Formal analysis, B.G., A.M.1, A.M.2, M.G.M., D.P., G.T.; Funding acquisition, B.G., A.S., I.M., G.T.; Investigation, B.G., A.M.1, A.M.2, M.G:M.;; Methodology, B.G., A.M.1, A.M.2, B.M., M.G.M.; Project administration, M.G.M, G.T.; Resources, A.S., I.M., G.T.; Software, B.G., A.M.1, M.G.M.; Supervision, A.M.2, B.M., D.P., M.G.M, G.T.; Validation, B.G., A.M.1, B.M., M.G.M.; Visualization, B.G., A.M.1, A.M.2, M.G.M.; Writing—Original Draft B.G., A.M.1, M.G.M.; Writing—Review & Editing, B.G., A.M.1, A.M.2, A.S, B.M., I.M., D.P., M.G.M., G.T. All authors have read and agreed to the published version of the manuscript.

Funding: This research did not receive any specific grant from funding agencies in the public, commercial, or not-for-profit sectors. We gratefully acknowledge the financial support provided by the EMBO Scientific Exchange Grant (number 10787), which facilitated collaboration with research groups and covered the travel and subsistence expenses of the first author, Benedetta Guagnini.

Institutional Review Board Statement: All animal procedures were conducted under the approval of the Cantonal Veterinary Office of Basel-Stadt (permit number BS 1797, and National no. 37404), in accordance with the Swiss Animal Welfare Act (TSchG, SR 455) and Ordinance (TSchV, SR 455.1), and in compliance with the 3Rs principles.

Informed Consent Statement: Informed consent was obtained under the general consent (Forschungskonsent) of the University Hospital Basel, approved by Swissethics (Art. 29, 32 Human Research Ordinance, HFV).

Data Availability Statement: The raw data supporting the conclusions of this article will be made available by the authors on request.

Acknowledgments: We want to thank the members of the Histology and Microscopy Core Facilities (Department of Biomedicine, University of Basel), and Susanne Erpel at the Nano Imaging Lab (SNI, University of Basel) for their support. We also extend our gratitude to Professor Devis Bellucci and Valeria Cannillo from the Department of Engineering "Enzo Ferrari," University of Modena and Reggio Emilia, for providing the BGMS10 bioactive glass used in this study. The authors acknowledge that this collaboration between the University of Trieste and the University of Basel originated from discussions at the TERMIS-EU Conference in Manchester (2023), which facilitated the exchange of ideas and expertise leading to this study.

Conflicts of Interest: The authors declare no conflicts of interest.

Abbreviations

The following abbreviations are used in this manuscript:

AL	alginate/hydroxyapatite scaffolds
Alg	alginate
ALP	alkaline phosphatase
ASCs	adipose-derived stromal cells
BG	AL scaffolds with bioactive glass
BGMS10	strontium/magnesium enriched bioactive glass
BM	bone marrow

 doi:10.20944/preprints202508.2185.v1

BM-MSCs	primary bone marrow-derived stromal cells
BSP	bone sialoprotein
CM	complete medium
COL1A1	collagen type I
FN	AL scaffolds with fibronectin
GDL	glucono-delta-lactone
HAp	hydroxyapatite
M-SOD	mesenchymal stromal cells sword of Damocles
OB	osteoblastic differentiation medium
OPN	osteopontin
PM	proliferation medium
RUNX2	Runt-related transcription factor 2
SEM	scanning electron microscopy
SVF	stromal vascular fraction

References

1. O'Brien, F.J. Biomaterials & Scaffolds for Tissue Engineering. Mater. Today 2011, 14, 88–95, doi:10.1016/S1369-7021(11)70058-X.
2. Turnbull, G.; Clarke, J.; Picard, F.; Riches, P.; Jia, L.; Han, F.; Li, B.; Shu, W. 3D Bioactive Composite Scaffolds for Bone Tissue Engineering. Bioact. Mater. 2018, 3, 278–314, doi:10.1016/j.bioactmat.2017.10.001.
3. Hurtado, A.; Aljabali, A.A.A.; Mishra, V.; Tambuwala, M.M.; Serrano-Aroca, Á. Alginate: Enhancement Strategies for Advanced Applications. Int. J. Mol. Sci. 2022, 23, 4486, doi:10.3390/ijms23094486.
4. Venkatesan, J.; Bhatnagar, I.; Manivasagan, P.; Kang, K.-H.; Kim, S.-K. Alginate Composites for Bone Tissue Engineering: A Review. Int. J. Biol. Macromol. 2015, 72, 269–281, doi:10.1016/j.ijbiomac.2014.07.008.
5. Hernández-González, A.C.; Téllez-Jurado, L.; Rodríguez-Lorenzo, L.M. Alginate Hydrogels for Bone Tissue Engineering, from Injectables to Bioprinting: A Review. Carbohydr. Polym. 2020, 229, 115514, doi:10.1016/j.carbpol.2019.115514.
6. Turco, G.; Marsich, E.; Bellomo, F.; Semeraro, S.; Donati, I.; Brun, F.; Grandolfo, M.; Accardo, A.; Paoletti, S. Alginate/Hydroxyapatite Biocomposite for Bone Ingrowth: A Trabecular Structure with High and Isotropic Connectivity. Biomacromolecules 2009, 10, 1575–1583, doi:10.1021/bm900154b.
7. Sancilio, S.; Gallorini, M.; Di Nisio, C.; Marsich, E.; Di Pietro, R.; Schweikl, H.; Cataldi, A. Alginate/Hydroxyapatite-Based Nanocomposite Scaffolds for Bone Tissue Engineering Improve Dental Pulp Biomineralization and Differentiation. Stem Cells Int. 2018, 2018, 13, doi:10.1155/2018/9643721.
8. Porrelli, D.; Gruppuso, M.; Vecchies, F.; Marsich, E.; Turco, G. Alginate Bone Scaffolds Coated with a Bioactive Lactose Modified Chitosan for Human Dental Pulp Stem Cells Proliferation and Differentiation. Carbohydr. Polym. 2021, 273, 118610, doi:10.1016/j.carbpol.2021.118610.
9. Rezwan, K.; Chen, Q.Z.; Blaker, J.J.; Boccaccini, A.R. Biodegradable and Bioactive Porous Polymer/Inorganic Composite Scaffolds for Bone Tissue Engineering. Biomaterials 2006, 27, 3413–3431, doi:10.1016/j.biomaterials.2006.01.039.
10. Bellucci, D.; Cannillo, V. A Novel Bioactive Glass Containing Strontium and Magnesium with Ultra-High Crystallization Temperature. Mater. Lett. 2018, 213, 67–70, doi:10.1016/j.matlet.2017.11.020.
11. Zumbo, B.; Guagnini, B.; Medagli, B.; Porrelli, D.; Turco, G. Fibronectin Functionalization: A Way to Enhance Dynamic Cell Culture on Alginate/Hydroxyapatite Scaffolds. J. Funct. Biomater. 2024, 15, 222, doi:10.3390/jfb15080222.
12. Guagnini, B.; Medagli, B.; Zumbo, B.; Cannillo, V.; Turco, G.; Porrelli, D.; Bellucci, D. Alginate-Sr/Mg Containing Bioactive Glass Scaffolds: The Characterization of a New 3D Composite for Bone Tissue Engineering. J. Funct. Biomater. 2024, 15, 183, doi:10.3390/jfb15070183.
13. Czekanska, E.M.; Stoddart, M.J.; Ralphs, J.R.; Richards, R.G.; Hayes, J.S. A Phenotypic Comparison of Osteoblast Cell Lines versus Human Primary Osteoblasts for Biomaterials Testing. J. Biomed. Mater. Res. A 2014, 102, 2636–2643, doi:10.1002/jbm.a.34937.
14. Hulsart-Billström, G.; Dawson, J.I.; Hofmann, S.; Müller, R.; Stoddart, M.J.; Alini, M.; Redl, H.; El Haj, A.; Brown, R.; Salih, V.; et al. A Surprisingly Poor Correlation between in Vitro and in Vivo Testing of

 doi:10.20944/preprints202508.2185.v1

Biomaterials for Bone Regeneration: Results of a Multicentre Analysis. Eur. Cell. Mater. 2016, 31, 312–322, doi:10.22203/ecm.v031a20.

15. Marolt, D.; Knezevic, M.; Novakovic, G.V. Bone Tissue Engineering with Human Stem Cells. Stem Cell Res. Ther. 2010, 1, 10, doi:10.1186/scrt10.
16. Scherberich, A.; Galli, R.; Jaquiery, C.; Farhadi, J.; Martin, I. Three-Dimensional Perfusion Culture of Human Adipose Tissue-Derived Endothelial and Osteoblastic Progenitors Generates Osteogenic Constructs with Intrinsic Vascularization Capacity. Stem Cells 2007, 25, 1823–1829, doi:10.1634/stemcells.2007-0124.
17. Bourgine, P.; Le Magnen, C.; Pigeot, S.; Geurts, J.; Scherberich, A.; Martin, I. Combination of Immortalization and Inducible Death Strategies to Generate a Human Mesenchymal Stromal Cell Line with Controlled Survival. Stem Cell Res. 2014, 12, 584–598, doi:10.1016/j.scr.2013.12.006.
18. Papadimitropoulos, A.; Scherberich, A.; Güven, S.; Theilgaard, N.; Crooijmans, H.J.A.; Santini, F.; Scheffler, K.; Zallone, A.; Martin, I. A 3D in Vitro Bone Organ Model Using Human Progenitor Cells. Eur. Cell Mater. 2011, 21, 445–458, doi:10.22203/ecm.v021a33.
19. Guerrero, J.; Pigeot, S.; Müller, J.; Schaefer, D.J.; Martin, I.; Scherberich, A. Fractionated Human Adipose Tissue as a Native Biomaterial for the Generation of a Bone Organ by Endochondral Ossification. Acta Biomater. 2018, 77, 142–154, doi:10.1016/j.actbio.2018.07.004.
20. Osinga, R.; Di Maggio, N.; Todorov, A.; Allafi, N.; Barbero, A.; Laurent, F.; Schaefer, D.J.; Martin, I.; Scherberich, A. Generation of a Bone Organ by Human Adipose-Derived Stromal Cells Through Endochondral Ossification. Stem Cells Transl. Med. 2016, 5, 1090–1097, doi:10.5966/sctm.2015-0256.
21. Perez, J.R.; Kouroupis, D.; Li, D.J.; Best, T.M.; Kaplan, L.; Correa, D. Tissue Engineering and Cell-Based Therapies for Fractures and Bone Defects. Front. Bioeng. Biotechnol. 2018, 6, 105, doi:10.3389/fbioe.2018.00105.
22. García, A.J.; Vega, M.D.; Boettiger, D. Modulation of Cell Proliferation and Differentiation through Substrate-Dependent Changes in Fibronectin Conformation. Mol. Biol. Cell. 1999, 10, 785–798, doi:10.1091/mbc.10.3.785.
23. García, A.J.; Reyes, C.D. Bio-Adhesive Surfaces to Promote Osteoblast Differentiation and Bone Formation. J. Dent. Res. 2005, 84, 407–413, doi:10.1177/154405910508400502.
24. Hench, L.L.; Polak, J.M. Third-Generation Biomedical Materials. Science 2002, 295, 1014–1017, doi:10.1126/science.1067404.
25. Gentile, P.; Mattioli-Belmonte, M.; Chiono, V.; Ferretti, C.; Baino, F.; Tonda-Turo, C.; Vitale-Brovarone, C.; Pashkuleva, I.; Reis, R.L.; Ciardelli, G. Bioactive Glass/Polymer Composite Scaffolds Mimicking Bone Tissue. J. Biomed. Mater. Res. A 2012, 100A, 2654–2667, doi:10.1002/jbm.a.34205.
26. Farzadi, A.; Bakhshi, F.; Solati-Hashjin, M.; Asadi-Eydivand, M.; Osman, N.A. abu Magnesium Incorporated Hydroxyapatite: Synthesis and Structural Properties Characterization. Ceram. Int. 2014, 40, 6021–6029, doi:10.1016/j.ceramint.2013.11.051.
27. Liu, J.; Rawlinson, S.C.F.; Hill, R.G.; Fortune, F. Strontium-Substituted Bioactive Glasses in Vitro Osteogenic and Antibacterial Effects. Dent. Mater. 2016, 32, 412–422, doi:10.1016/j.dental.2015.12.013.
28. Mahmoud, E.M.; Sayed, M.; El-Kady, A.M.; Elsayed, H.; Naga, S.M. In Vitro and in Vivo Study of Naturally Derived Alginate/Hydroxyapatite Bio Composite Scaffolds. Int. J. Biol. Macromol. 2020, 165, 1346–1360, doi:10.1016/j.ijbiomac.2020.10.014.
29. Przekora, A. The Summary of the Most Important Cell-Biomaterial Interactions That Need to Be Considered during in Vitro Biocompatibility Testing of Bone Scaffolds for Tissue Engineering Applications. Mater. Sci. Eng. C 2019, 97, 1036–1051, doi:10.1016/j.msec.2019.01.061.
30. Kruyt, M.C.; Dhert, W.J.A.; Yuan, H.; Wilson, C.E.; van Blitterswijk, C.A.; Verbout, A.J.; de Bruijn, J.D. Bone Tissue Engineering in a Critical Size Defect Compared to Ectopic Implantations in the Goat. J. Orthop. Res. 2004, 22, 544–551, doi:10.1016/j.orthres.2003.10.010.
31. Poh, P.S.P.; Hutmacher, D.W.; Holzapfel, B.M.; Solanki, A.K.; Stevens, M.M.; Woodruff, M.A. In Vitro and in Vivo Bone Formation Potential of Surface Calcium Phosphate-Coated Polycaprolactone and Polycaprolactone/Bioactive Glass Composite Scaffolds. Acta Biomater. 2016, 30, 319–333, doi:10.1016/j.actbio.2015.11.012.

 doi:10.20944/preprints202508.2185.v1

32. Causa, F.; Netti, P.A.; Ambrosio, L. A Multi-Functional Scaffold for Tissue Regeneration: The Need to Engineer a Tissue Analogue. Biomaterials 2007, 28, 5093–5099, doi:10.1016/j.biomaterials.2007.07.030.
33. Gentile, P.; Mattioli-Belmonte, M.; Chiono, V.; Ferretti, C.; Baino, F.; Tonda-Turo, C.; Vitale-Brovarone, C.; Pashkuleva, I.; Reis, R.L.; Ciardelli, G. Bioactive Glass/Polymer Composite Scaffolds Mimicking Bone Tissue. J. Biomed. Mater. Res. A 2012, 100A, 2654–2667, doi:10.1002/jbm.a.34205.
34. Masson-Meyers, D.S.; Tayebi, L. Vascularization Strategies in Tissue Engineering Approaches for Soft Tissue Repair. J. Tissue Eng. Regen. Med. 2021, 15, 747–762, doi:10.1002/term.3225.
35. Zhao, F.; van Rietbergen, B.; Ito, K.; Hofmann, S. Flow Rates in Perfusion Bioreactors to Maximise Mineralisation in Bone Tissue Engineering in Vitro. J. Biomech. 2018, 79, 232–237, doi:10.1016/j.jbiomech.2018.08.004.
36. Muschler, G.F.; Raut, V.P.; Patterson, T.E.; Wenke, J.C.; Hollinger, J.O. The Design and Use of Animal Models for Translational Research in Bone Tissue Engineering and Regenerative Medicine. Tissue Eng. Part B Rev. 2010, 16(1), 123-45. doi: 10.1089/ten.TEB.2009.0658. Author 1, A.; Author 2, B. Title of the chapter. In *Book Title*, 2nd ed.; Editor 1, A., Editor 2, B., Eds.; Publisher: Publisher Location, Country, 2007; Volume 3, pp. 154–196.